Enhanced Quantum Interface with Collective Ion-Cavity Coupling

B. Casabone,[1] K. Friebe,[1] B. Brandstätter,[1] K. Schüppert,[1] R. Blatt,[1,2] and T. E. Northup[1,*]
[1]Institut für Experimentalphysik, Universität Innsbruck, Technikerstraße 25, 6020 Innsbruck, Austria
[2]Institut für Quantenoptik und Quanteninformation, Österreichische Akademie der Wissenschaften, Technikerstraße 21a, 6020 Innsbruck, Austria

(Received 26 August 2014; published 14 January 2015)

We prepare a maximally entangled state of two ions and couple both ions to the mode of an optical cavity. The phase of the entangled state determines the collective interaction of the ions with the cavity mode, that is, whether the emission of a single photon into the cavity is suppressed or enhanced. By adjusting this phase, we tune the ion-cavity system from sub- to superradiance. We then encode a single qubit in the two-ion superradiant state and show that this encoding enhances the transfer of quantum information onto a photon.

DOI: 10.1103/PhysRevLett.114.023602 PACS numbers: 42.50.Nn, 42.50.Dv, 42.50.Pq

Sub- and superradiance are fundamental effects in quantum optics arising in systems that are symmetric under the interchange of any pair of particles [1–3]. Superradiance has been widely studied in many-atom systems, in which effects such as a phase transition [4,5] and narrow-linewidth lasing [6] have recently been observed. For few-atom systems, each atom's state and position can be precisely controlled, and thus collective emission effects such as Rydberg blockade [7] and the Lamb shift [8] can be tailored. In a pioneering experiment using two trapped ions, variation of the ions' separation allowed both sub- and superradiance to be observed, with the excited-state lifetime extended or reduced by up to 1.5% [9]. The contrast was limited because spontaneous emission from the ions was not indistinguishable, as the ions' separation was on the order of the wavelength of the emitted radiation. This limitation can be overcome by observing preferential emission into a single mode, such as the mode defined by incident radiation [1] or by an optical cavity. In a cavity setting, indistinguishability is guaranteed when the emitters are equally coupled to the mode, even if they are spatially separated. Subradiance corresponds to a suppressed interaction of the joint state of the emitters with the cavity mode, while for the superradiant state, the interaction is enhanced.

In the context of quantum networks [10,11], superradiance can improve a quantum interface when one logical qubit is encoded across N physical qubits. In the Duan-Lukin-Cirac-Zoller protocol for heralded remote entanglement, efficient retrieval of stored photons is based on superradiance [12,13]. Superradiance can also improve the performance of a deterministic, cavity-based interface, which enables the direct transmission of quantum information between network nodes [14]. If a qubit is encoded in the state $1/\sqrt{N}\sum_i^N |\downarrow_1 \ldots \uparrow_i \ldots \downarrow_N\rangle$, the coupling rate to the cavity is enhanced from the single-qubit rate g to the effective rate $g\sqrt{N}$, relaxing the technical requirements for strong coupling between light and matter [15]. This state corresponds to the first step in the superradiant cascade described by Dicke [1]. In contrast, subradiant states are antisymmetrized, resulting in suppressed emission. From a quantum-information perspective, subradiant states are interesting because they span a decoherence-free subspace [16–18]. A subradiant state of two superconducting qubits coupled to a cavity has recently been prepared [19].

Here, we generate collective states of two ions coupled to an optical cavity and use a state that maximizes the coupling rate to improve ion-photon quantum information transfer. Our system is described by the Tavis-Cummings Hamiltonian [20], the interaction term of which is

$$H_{\mathrm{int}} = \hbar g(\sigma_-^{(1)} + e^{i\zeta}\sigma_-^{(2)})a^\dagger + \mathrm{H.c.}, \tag{1}$$

where $\sigma_-^{(j)}$ is the lowering operator for the jth ion, ζ represents a relative phase [21], and $a^\dagger$ is the creation operator of a photon in the cavity mode. We prepare a maximally entangled two-ion state and tune its emission properties between sub- and superradiance, that is, between a dark state $|\Psi_{\mathrm{sub}}\rangle$ and a state $|\Psi_{\mathrm{super}}\rangle$ that couples with enhanced strength $g\sqrt{2}$ to the cavity. Furthermore, we transfer quantum information from a state with enhanced emission probability onto a single photon and show that the process fidelity and efficiency are higher than for a single-ion qubit.

In these experiments, two $^{40}Ca^+$ separated by 5.6 μm are confined along the axis of a linear Paul trap and coupled to an optical cavity in an intermediate coupling regime [21]. We position the ions so that $g_1 \approx g_2$, where g_j represents the coupling strength of the jth ion to the cavity [25]. In a cavity-mediated Raman process, each ion prepared in a state from the $4^2S_{1/2}$ manifold produces a single cavity photon [26]. The process is driven both by a laser at 393 nm detuned from the $4^2S_{1/2} - 4^2P_{3/2}$ transition and by the cavity, whose detuning from the 854 nm $4^2P_{3/2} - 3^2D_{5/2}$ transition satisfies a Raman resonance condition [27].

Together, laser and cavity provide the interaction term of Eq. (1), in which the relative phase ζ between the ions' coupling arises from the angle between the Raman beam and the ion-trap axis [21]. Photons leave the cavity preferentially through one mirror and are detected on photodiodes [Fig. 1(a)].

Entanglement between the ions is generated using a "global" 729 nm laser beam [Fig. 1(a)] that couples with equal strength to both ions on the $4^2S_{1/2} - 3^2D_{5/2}$ quadrupole transition. The target state

$$|\Psi^+\rangle \equiv (|S\rangle|D\rangle + |D\rangle|S\rangle)/\sqrt{2}$$

is prepared via a Mølmer-Sørensen gate operation followed by a $\pi/2$ rotation, where $|S\rangle \equiv |4^2S_{1/2}, m_j = -1/2\rangle$ and $|D\rangle \equiv |3^2D_{5/2}, m_j = -1/2\rangle$. In the Mølmer-Sørensen gate, a bichromatic field that drives blue and red motional sidebands generates a spin-dependent force, coupling the

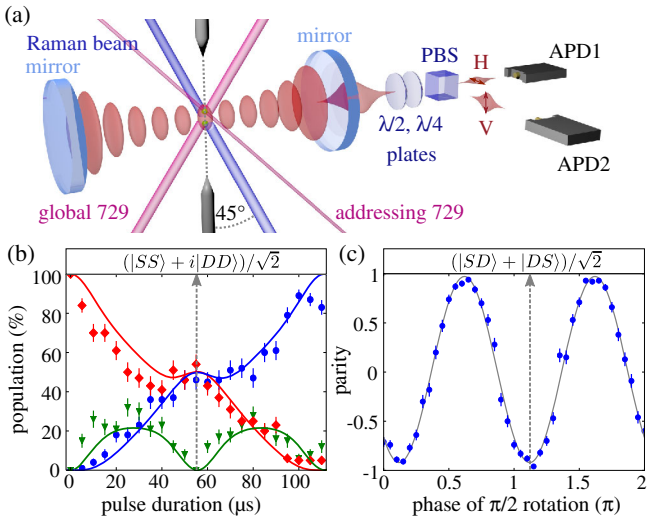

FIG. 1 (color online). (a) Two $^{40}Ca^+$ ions in a linear Paul trap couple with equal strength to the mode of a high-finesse optical cavity. A magnetic field orthogonal to the cavity axis defines the quantization axis. Quantum information stored in the ions is manipulated using two 729 nm beams: the global beam couples to both ions, while the addressing beam is focused onto one ion. A 393 nm laser beam drives a cavity-mediated Raman transition, generating a single photon in the cavity. At the cavity output, two wave plates ($\lambda/2$, $\lambda/4$) select the basis in which photon polarization is analyzed. Two avalanche photodiodes (APD1 and APD2) detect the horizontally (H) or vertically (V) polarized photons at the output of a polarizing beam splitter (PBS). (b) Populations of the states $|S\rangle|S\rangle$ (red diamonds), $|D\rangle|D\rangle$ (blue circles), and $|S\rangle|D\rangle$ or $|D\rangle|S\rangle$ (green triangles) as a function of the Mølmer–Sørensen gate duration. After 55 μs (dashed vertical line) a maximally entangled state is generated. Solid lines indicate the ideal time evolution of the gate operation [28]. (c) Oscillations in the parity of the ion populations as a function of the phase of a $\pi/2$ pulse on the $|S\rangle \leftrightarrow |D\rangle$ transition, following entanglement. The dashed vertical line at phase 1.2π corresponds to $|\Psi^+\rangle$. Error bars represent projection noise.

ion's motion and internal state [29]. Figure 1(b) shows the evolution of the two-ion state populations during application of the gate. A maximally entangled state $|\Phi\rangle = (|S\rangle|S\rangle + i|D\rangle|D\rangle)/\sqrt{2}$ is generated for a gate duration of 55 μs. Subsequently, a $\pi/2$ rotation maps $|\Phi\rangle$ to $|\Psi^+\rangle$. A lower bound of 95(2)% on the state fidelity with respect to $|\Phi\rangle$ is determined by varying the phase of the $\pi/2$ rotation and measuring the parity of the ions' populations, which oscillates as a function of phase [Fig. 1(c)] [30].

A second, "addressing" 729 nm beam with a waist smaller than the ion-ion separation couples to just one ion. When detuned, this beam induces ac-Stark shifts in the addressed ion, which contribute a phase φ to the entangled state [31]:

$$|\Psi(\varphi)\rangle \equiv (|S\rangle|D\rangle + e^{i\varphi}|D\rangle|S\rangle)/\sqrt{2}. \quad (2)$$

By adjusting the length of the Stark-shift pulse, we shift this phase, which determines the effective coupling g_{eff} of $|\Psi(\varphi)\rangle$ to the cavity mode under the action of H_{int}. Specifically, the superradiant and subradiant states are given by

$$|\Psi_{\text{super}}\rangle \equiv |\Psi(\varphi = -\zeta)\rangle,$$
$$|\Psi_{\text{sub}}\rangle \equiv |\Psi(\varphi = -\zeta + \pi)\rangle. \quad (3)$$

Note that if ζ were zero, $|\Psi_{\text{super}}\rangle$ and $|\Psi_{\text{sub}}\rangle$ would be the Bell states $|\Psi^+\rangle$ and $|\Psi^-\rangle$, respectively.

The Raman process between $|S\rangle$ and $|D\rangle$ generates a single cavity photon from $|\Psi(\varphi)\rangle$, as only one ion is in $|S\rangle$. This photon has a temporal shape initially determined by g_{eff} between the two-ion state and the cavity mode. For later times, the shape is determined by the rates of both cavity decay and off-resonant scattering. Varying g_{eff} by changing the phase φ of $|\Psi(\varphi)\rangle$ thus modifies the temporal shape, that is, the probability to generate the photon early in the Raman process. Ideally, in the absence of scattering, the coupling of $|\Psi_{\text{sub}}\rangle$ to the cavity vanishes ($g_{\text{eff}} = 0$) so that no photon is generated. For $|\Psi_{\text{super}}\rangle$, in contrast, the coupling is maximized such that $g_{\text{eff}} = g\sqrt{2}$. Thus, the probability to generate and detect a photon from $|\Psi_{\text{super}}\rangle$ early in the process is expected to be twice that of one ion. For time scales much shorter than $1/g$, a photon generated in the cavity has not yet been reabsorbed, and therefore, cavity backaction does not play a role.

We now determine this probability for a range of phases φ. The experimental sequence starts with 1 ms of Doppler cooling. The ions are then optically pumped to $|S\rangle$, followed by 1.3 ms of sideband cooling on the axial center-of-mass mode [32]. Next, global and addressing 729 nm pulses generate the state $|\Psi(\varphi)\rangle$. In the last step, the cavity-mediated Raman transition is driven for 55 μs and photons are detected [Fig. 2(a)].

In order to determine whether we achieve enhancement and suppression of the cavity coupling with respect to the

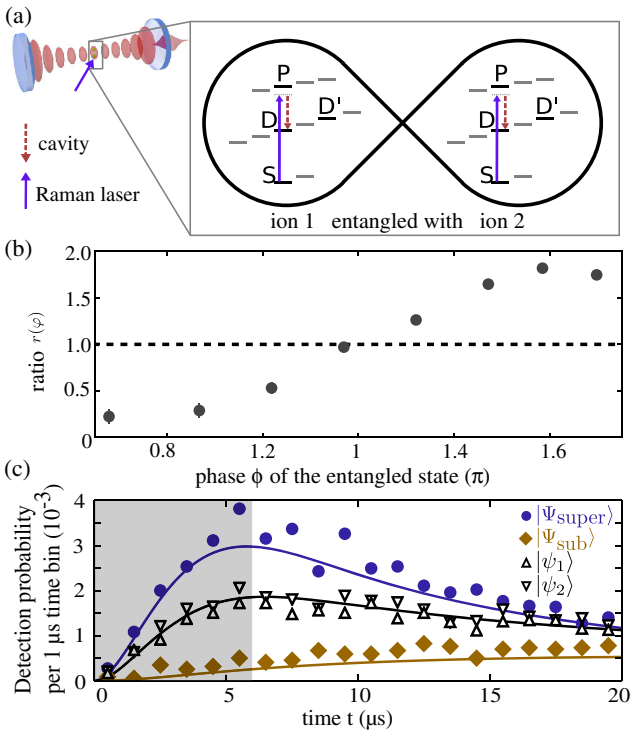

FIG. 2 (color online). (a) The two ions are prepared in either a separable state $|\psi_1\rangle$ or $|\psi_2\rangle$ or an entangled state $|\Psi(\varphi)\rangle$ for various values of φ. The global beam then drives a Raman transition between $|S\rangle$ and $|D\rangle$, generating a single cavity photon for each ion in $|S\rangle$. Since $|D'\rangle$ is decoupled from the cavity interaction, both $|\psi_1\rangle$ and $|\psi_2\rangle$ represent a single ion interacting with the cavity. (b) Ratio $r(\varphi)$ of the probability to detect a photon for $|\Psi(\varphi)\rangle$ to that of $|\psi_1\rangle$ as a function of the phase φ for the first 6 μs of the Raman process. The reference single-ion case is shown as a dashed horizontal line. (c) Temporal shape of the photon at the cavity output as a function of detection time t, for the entangled states $|\Psi_{\text{super}}\rangle$ (circles) and $|\Psi_{\text{sub}}\rangle$ (diamonds) and the single-ion cases $|\psi_1\rangle$ and $|\psi_2\rangle$ (up and down triangles, respectively). The temporal photon shapes are calculated by normalizing the detected photon counts per 1 μs time bin by the number of photon generation attempts. Data are shown until 20 μs, the time scale for which enhancement and suppression are most prominent. Lines are simulations. The shaded area represents the time window used in (b). Error bars represent Poissonian statistics and are mostly smaller than the plot symbols.

single-ion rate g, we carry out a reference measurement. For this single-ion case, one of the two ions is hidden in a state $|D'\rangle \equiv |3^2D_{5/2}, m_j = 3/2\rangle$ that is decoupled from the Raman process. Thus, the initial state is $|\psi_1\rangle \equiv |S\rangle|D'\rangle$ or $|\psi_2\rangle \equiv |D'\rangle|S\rangle$.

For the states $|\Psi(\varphi)\rangle$, we calculate $\eta(\varphi)$, the probability to detect a photon in the first 6 μs of the Raman process, an interval in which the effective coupling rate determines the initial slope. For the single-ion cases, we calculate η_ψ, the average value of the photon detection probability for $|\psi_1\rangle$ and $|\psi_2\rangle$ in the same time window. Figure 2(b) shows the ratio $r(\varphi) = \eta(\varphi)/\eta_\psi$ as the phase φ is varied. For $\varphi = 0.68\pi$, the experimentally determined minimum, the ratio is 0.22(9): photon generation is strongly suppressed. We therefore identify $|\Psi(\varphi = 0.68\pi)\rangle$ with $|\Psi_{\text{sub}}\rangle$. As φ is increased, the ratio approaches one, then enters the superradiant regime. A maximum value of $r(\varphi)$ is found for $\varphi = 1.58\pi$. For the corresponding state, identified with $|\Psi_{\text{super}}\rangle$, the probability to detect a photon is 1.84(4), close to its maximum value of 2, thus demonstrating strong enhancement in photon generation.

For these states $|\Psi_{\text{sub}}\rangle$ and $|\Psi_{\text{super}}\rangle$, we now analyze the temporal photon shapes at the detector [Fig. 2(c)]. The temporal shapes corresponding to $|\psi_1\rangle$ and $|\psi_2\rangle$ are considered as a reference; from their overlap, we find the coupling strengths of the two ions, g_1 and g_2, to be within 10% of one another. Photons generated from $|\Psi_{\text{super}}\rangle$ exhibit a steeper initial slope than the single-ion case, while $|\Psi_{\text{sub}}\rangle$ has a flatter slope. The photon shapes are consistent with enhanced and suppressed coupling to the cavity and are in good agreement with simulations. The simulations are based on numerical integration of the master equation and include imperfect preparation of the initial state, which together with off-resonant scattering accounts for the small but nonzero probability to generate photons from $|\Psi_{\text{sub}}\rangle$. For $|\Psi_{\text{super}}\rangle$, these effects reduce the photon generation probability by about 10% for the first 6 μs of the process [21].

We now describe the implementation of a quantum interface that exploits the enhanced coupling of the superradiant state to the cavity [15]. The state $|\Psi(\varphi)\rangle$ as defined in Eq. (2) contains two contributions: one from the ground state $|S\rangle$ and the other from $|D\rangle$. We extend this definition so that the ground-state component can be stored in either of two states, that is, in $|S\rangle$ or in $|S'\rangle \equiv |4^2S_{1/2}, m_j = +1/2\rangle$. A logical qubit is encoded in these two states, and this qubit is mapped onto the polarization state of a single cavity photon. To perform the mapping process, we use a phase-stable bichromatic Raman transition that coherently transfers $|S\rangle$ to $|D\rangle$, producing a horizontally polarized photon $|H\rangle$, and $|S'\rangle$ to $|D\rangle$, producing a vertically polarized photon $|V\rangle$ [33] [Fig. 3(a)]. Defining a superposition state

$$|\alpha, \beta\rangle \equiv \cos\alpha|S\rangle + e^{i\beta}\sin\alpha|S'\rangle,$$

the mapping process can be represented by

$$\begin{aligned}(|\alpha,\beta\rangle|D\rangle + e^{i\varphi}|D\rangle|\alpha,\beta\rangle)|0\rangle/\sqrt{2} \\ \mapsto |D\rangle|D\rangle(\cos\alpha|H\rangle + e^{i\beta}\sin\alpha|V\rangle),\end{aligned} \tag{4}$$

where $|0\rangle$ stands for the cavity vacuum and the phase is set to $\varphi = 1.58\pi$, corresponding to $|\Psi_{\text{super}}\rangle$.

In order to characterize the mapping, we extract the process matrix χ, which describes the transformation from the input to the output density matrix: $\rho_{\text{out}} = \sum_{i,j}\chi_{ij}\sigma_i\rho_{\text{in}}\sigma_j$, where $\sigma_i \in \{\mathbb{1}, \sigma_x, \sigma_y, \sigma_z\}$ are the Pauli operators [34]. Following Doppler cooling, optical pumping, and sideband

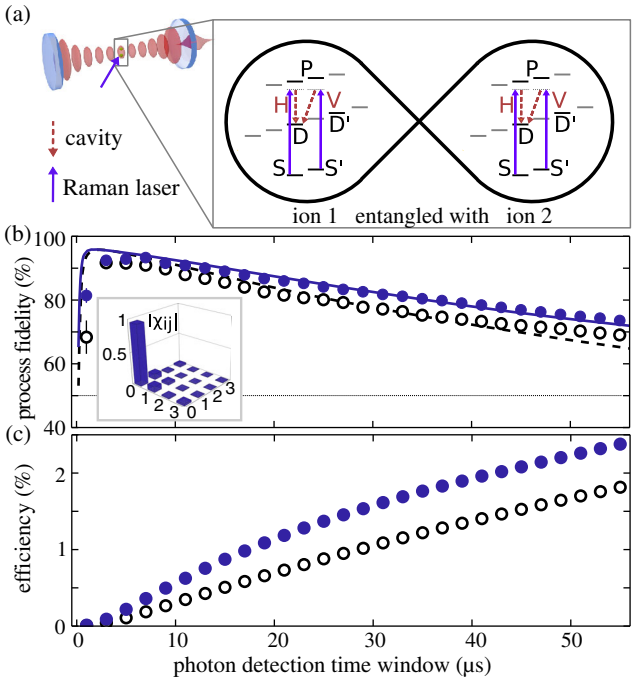

FIG. 3 (color online). (a) A bichromatic Raman transition maps a superposition of $|S\rangle$ and $|S'\rangle$ onto a superposition of single-photon polarization states $|H\rangle$ and $|V\rangle$. The superposition is encoded either in two entangled ions or in a single ion, with the other ion decoupled in $|D'\rangle$. (b) Process fidelity for $|\Psi_{\mathrm{super}}\rangle$ (filled blue circles) and $|\psi_1\rangle$ (open black circles) as a function of the photon detection time window. Lines are simulations (continuous line: two entangled ions; dashed line: single-ion case). Inset: absolute value of the process matrix χ_{ij} for $|\Psi_{\mathrm{super}}\rangle$ reconstructed from photons detected between 2 and 4 μs, yielding the maximum process fidelity $|\chi_{00}| = 96.0(3)\%$. Error bars are derived from nonparametric bootstrapping. (c) Cumulative process efficiency for $|\Psi_{\mathrm{super}}\rangle$ (filled blue circles) and $|\psi_1\rangle$ (open black circles) as a function of the photon detection time window. Error bars represent Poissonian statistics and are smaller than the plot symbols.

cooling as above, the two ions are prepared in $|\Psi_{\mathrm{super}}\rangle$. Next, two global 729 nm pulses prepare one of the four orthogonal input states $|\alpha,\beta\rangle$, with $(\alpha,\beta) \in \{(\pi/2,0), (0,0), (\pi/4,0), (\pi/4,\pi/2)\}$. Finally, the Raman transition is driven and the photon is detected in one of three orthogonal polarization bases [35]. This set of measurements allows χ to be reconstructed via the maximum likelihood method. As the target mapping corresponds to the identity operation, the process fidelity is given by the matrix entry χ_{00}.

For comparison, we carry out reference measurements in which enhancement is not present, for which the ions are prepared in $|\psi_1\rangle$. The mapping process is then given by

$$|\alpha,\beta\rangle|D'\rangle|0\rangle \mapsto |D\rangle|D'\rangle(\cos\alpha|H\rangle + e^{i\beta}\sin\alpha|V\rangle).$$

Figure 3(b) shows the process fidelities χ_{00} for $|\Psi_{\mathrm{super}}\rangle$ and $|\psi_1\rangle$ as a function of the photon detection time window. Not only is the fidelity of the superradiant case higher for all data points, but also the improvement over the single-ion case increases with the length of the detection window. For a detection time window of 6 μs, the fidelity is 93.3(3)% for $|\Psi_{\mathrm{super}}\rangle$ and 90.9(5)% for $|\psi_1\rangle$, indicating that in both cases the logical qubit is correctly mapped onto photon polarization with very high probability. A maximum value of 96.0(3)% is found for $|\Psi_{\mathrm{super}}\rangle$ for photons detected between 2 and 4 μs. As the detection window length is increased, χ_{00} decreases for both cases because the probability for off-resonant excitation to the $4^2P_{3/2}$ manifold increases with time. If such an event happens during the Raman process, the initial state $|\alpha,\beta\rangle$ is randomly projected onto $|0,0\rangle = |S\rangle$ or $|\pi/2,0\rangle = |S'\rangle$, and the qubit is then mapped onto either $|H\rangle$ or $|V\rangle$, regardless of the information in the initial superposition [33]. However, while the probability for scattering is the same for both states, photons are produced earlier from $|\Psi_{\mathrm{super}}\rangle$ because of the enhanced effective coupling. Thus, the improvement in the fidelity stems from an increased probability to generate a photon before scattering occurs. After 55 μs, we find $\chi_{00} = 73.4(3)\%$ for $|\Psi_{\mathrm{super}}\rangle$ in comparison with 68.7(2)% for $|\psi_1\rangle$. Simulations that take into account detector dark counts, imperfect state initialization, different coupling strengths of the ions to the cavity, and magnetic field fluctuations are in good agreement with the data.

We also investigate the cumulative process efficiency $\varepsilon(t)$, defined as the probability to detect a photon before time t [Fig. 3(c)]. For $t = 6$ μs, the process efficiency for $|\Psi_{\mathrm{super}}\rangle$ is $\varepsilon_s(t) = 0.33(1)\%$, while for $|\psi_1\rangle$, it is $\varepsilon_1(t) = 0.17(1)\%$, corresponding to a ratio $\varepsilon_s/\varepsilon_1$ of 1.94 (13). The ratio decreases monotonically with t, and by $t = 55$ μs, it is 1.34(5). While the enhanced coupling modifies the temporal shape of the photons early in the process, for longer times its effect on the cumulative process efficiency is small, such that the ratio is expected to approach one. A single photon generated in the cavity is detected with an efficiency of 8(1)%, due to losses in the cavity mirrors, optical path losses and the detection efficiency of the avalanche photodiodes.

The enhanced fidelity and efficiency of quantum state transfer in the superradiant regime can be understood in terms of a stronger effective ion-cavity coupling. Further improvements are thus expected by encoding the logical qubit across more physical qubits, as in a planar microfabricated trap [36]. Maximum enhancement would be achieved by encoding not just one but $N/2$ excitations in a symmetrized N-ion state. The cooperative emission rate would then be $g\sqrt{N/2((N/2)+1)}$, which scales with N for large N, as observed in atomic ensembles [4–6]. However, it remains an open question how to transfer quantum information between such states and single photons, as required for a quantum transducer [15].

Finally, we emphasize two advantages of ions as qubits in these experiments: first, that the coupling strength of

each ion to the cavity can be precisely controlled, and second, that a universal set of gate operations [37] allows preparation of a range of states, from sub- to superradiant. By tuning over this range, one could selectively turn off and on the coupling of logical qubits to the cavity. This technique would provide a versatile tool for addressable read-write operations in a quantum register.

We thank L. Lamata and F. Ong for helpful discussions and A. Stute for early contributions to the experiment design. We gratefully acknowledge support from the Austrian Science Fund (FWF): Projects No. F4003, No. F4019, and No. V252, the European Commission via the Atomic QUantum TEchnologies (AQUTE) Integrating Project, and the Institut für Quanteninformation GmbH.

Note added.—Recently we learned of related work with two neutral atoms coupled to a cavity [38].

*Corresponding author.
tracy.northup@uibk.ac.at

[1] R. H. Dicke, Phys. Rev. **93**, 99 (1954).
[2] M. Gross and S. Haroche, Phys. Rep. **93**, 301 (1982).
[3] B. M. Garraway, Phil. Trans. R. Soc. A **369**, 1137 (2011).
[4] K. Baumann, C. Guerlin, F. Brennecke, and T. Esslinger, Nature (London) **464**, 1301 (2010).
[5] M. P. Baden, K. J. Arnold, A. L. Grimsmo, S. Parkins, and M. D. Barrett, Phys. Rev. Lett. **113**, 020408 (2014).
[6] J. G. Bohnet, Z. Chen, J. M. Weiner, D. Meiser, M. J. Holland, and J. K. Thompson, Nature (London) **484**, 78 (2012).
[7] M. D. Lukin, M. Fleischhauer, R. Cote, L. M. Duan, D. Jaksch, J. I. Cirac, and P. Zoller, Phys. Rev. Lett. **87**, 037901 (2001).
[8] Z. Meir, O. Schwartz, E. Shahmoon, D. Oron, and R. Ozeri, Phys. Rev. Lett. **113**, 193002 (2014).
[9] R. G. DeVoe and R. G. Brewer, Phys. Rev. Lett. **76**, 2049 (1996).
[10] H. J. Kimble, Nature (London) **453**, 1023 (2008).
[11] L.-M. Duan and C. Monroe, Rev. Mod. Phys. **82**, 1209 (2010).
[12] L.-M. Duan, M. D. Lukin, J. I. Cirac, and P. Zoller, Nature (London) **414**, 413 (2001).
[13] R. A. de Oliveira, M. S. Mendes, W. S. Martins, P. L. Saldanha, J. W. R. Tabosa, and D. Felinto, Phys. Rev. A **90**, 023848 (2014).
[14] J. I. Cirac, P. Zoller, H. J. Kimble, and H. Mabuchi, Phys. Rev. Lett. **78**, 3221 (1997).
[15] L. Lamata, D. R. Leibrandt, I. L. Chuang, J. I. Cirac, M. D. Lukin, V. Vuletić, and S. F. Yelin, Phys. Rev. Lett. **107**, 030501 (2011).
[16] M. B. Plenio, S. F. Huelga, A. Beige, and P. L. Knight, Phys. Rev. A **59**, 2468 (1999).
[17] A. Beige, D. Braun, B. Tregenna, and P. L. Knight, Phys. Rev. Lett. **85**, 1762 (2000).
[18] D. A. Lidar and K. Birgitta Whaley, in *Irreversible Quantum Dynamics*, Lecture Notes in Physics, Vol. 622, edited by F. Benatti and R. Floreanini (Springer, Berlin, Heidelberg, 2003) p. 83.
[19] S. Filipp, A. F. van Loo, M. Baur, L. Steffen, and A. Wallraff, Phys. Rev. A **84**, 061805 (2011).
[20] M. Tavis and F. W. Cummings, Phys. Rev. **170**, 379 (1968).
[21] See Supplemental Material at http://link.aps.org/supplemental/10.1103/PhysRevLett.114.023602, which includes Refs. [23–25], for details about the relative Raman phase, cavity coupling parameters, ion-ion entanglement, and simulations.
[22] M. A. Nielsen and I. L. Chuang, *Quantum Computation and Quantum Information* (Cambridge University Press, Cambridge, England, 2010).
[23] B. Efron and R. Tibshirani, *An Introduction to the Bootstrap* (Chapman & Hall, New York, 1993).
[24] S. M. Tan, J. Opt. B **1**, 424 (1999).
[25] B. Casabone, A. Stute, K. Friebe, B. Brandstätter, K. Schüppert, R. Blatt, and T. E. Northup, Phys. Rev. Lett. **111**, 100505 (2013).
[26] H. G. Barros, A. Stute, T. E. Northup, C. Russo, P. O. Schmidt, and R. Blatt, New J. Phys. **11**, 103004 (2009).
[27] A. Stute, B. Casabone, B. Brandstätter, D. Habicher, P. O. Schmidt, T. E. Northup, and R. Blatt, Appl. Phys. B **107**, 1145 (2012).
[28] J. Benhelm, G. Kirchmair, C. F. Roos, and R. Blatt, Nat. Phys. **4**, 463 (2008).
[29] A. Sørensen and K. Mølmer, Phys. Rev. Lett. **82**, 1971 (1999).
[30] C. Sackett, D. Kielpinski, B. King, C. Langer, V. Meyer, C. Myatt, M. Rowe, Q. Turchette, W. Itano, D. Wineland *et al.*, Nature (London) **404**, 256 (2000).
[31] P. Schindler, D. Nigg, T. Monz, J. T. Barreiro, E. Martinez, S. X. Wang, S. Quint, M. F. Brandl, V. Nebendahl, C. F. Roos *et al.*, New J. Phys. **15**, 123012 (2013).
[32] D. J. Wineland, C. Monroe, W. M. Itano, D. Leibfried, B. E. King, and D. M. Meekhof, J. Res. Natl. Inst. Stand. Technol. **103**, 259 (1998).
[33] A. Stute, B. Casabone, B. Brandstätter, K. Friebe, T. E. Northup, and R. Blatt, Nat. Photonics **7**, 219 (2013).
[34] I. L. Chuang and M. A. Nielsen, J. Mod. Opt. **44**, 2455 (1997).
[35] D. F. V. James, P. G. Kwiat, W. J. Munro, and A. G. White, Phys. Rev. A **64**, 052312 (2001).
[36] M. Cetina, A. Bylinskii, L. Karpa, D. Gangloff, K. M. Beck, Y. Ge, M. Scholz, A. T. Grier, I. Chuang, and V. Vuletić, New J. Phys. **15**, 053001 (2013).
[37] H. Häffner, C. Roos, and R. Blatt, Phys. Rep. **469**, 155 (2008).
[38] R. Reimann, W. Alt, T. Kampschulte, T. Macha, L. Ratschbacher, N. Thau, S. Yoon, and D. Meschede, preceding Letter, Phys. Rev. Lett. **114**, 023601 (2015).